Correlation between Lung Fibrosis and Radiation Therapy Dose after Concurrent Radiation Therapy and Chemotherapy for Limited Small Cell Lung Cancer[1]

Isaac I. Rosen, PhD
Teresa A. Fischer, MS
John A. Antolak, PhD
George Starkschall, PhD
Elizabeth L. Travis, PhD
Susan L. Tucker, PhD
Kenneth R. Hogstrom, PhD
James D. Cox, MD
Ritsuko Komaki, MD

Index terms:
Chemotherapy, complications, 60.47
Lung, fibrosis, 60.47
Radiations, injurious effects, 60.47

Published online before print
10.1148/radiol.2213992043
Radiology 2001; 221:614–622

Abbreviations:
AP-PA = anteroposterior-posteroanterior
PE = cisplatin and etoposide
PIE = cisplatin, ifosfamide, and etoposide
RTOG = Radiation Therapy Oncology Group
3D = three-dimensional
TP = treatment planning

[1] From the Departments of Radiation Physics (I.I.R., J.A.A., G.S., K.R.H.), Experimental Radiation Oncology (E.L.T.), Biomathematics (S.L.T.), and Radiation Oncology (J.D.C., R.K.), University of Texas M.D. Anderson Cancer Center, 1515 Holcombe Blvd, Box 94, Houston, TX 77030; and the Sarasota Radiation Therapy Regional Center, Sarasota, Fla (T.A.F.). From the 1998 RSNA scientific assembly. Received November 24, 1999; revision requested March 8, 2001; final revision received May 2; accepted May 21. **Address correspondence to** I.I.R. (e-mail: *irosen@mdanderson.org*).

Author contributions:
Guarantors of integrity of entire study, I.I.R., R.K.; study concepts and design, all authors; literature research, T.A.F., R.K.; clinical studies, R.K.; data acquisition, T.A.F., R.K.; data analysis/interpretation, T.A.F., I.I.R.; statistical analysis, I.I.R., S.L.T., T.A.F.; manuscript preparation, T.A.F., I.I.R.; manuscript definition of intellectual content, all authors; manuscript editing, revision/review, final version approval, I.I.R.

PURPOSE: To evaluate the relationship between physician-identified radiographic fibrosis, lung tissue physical density change, and radiation dose after concurrent radiation therapy and chemotherapy for limited small cell lung cancer.

MATERIALS AND METHODS: Fibrosis volumes of different severity levels were delineated on computed tomography (CT) images obtained at 1-year follow-up of 21 patients with complete response to concurrent radiation therapy and chemotherapy for limited small cell lung carcinoma. Delivered treatments were reconstructed with a three-dimensional treatment planning system and geometrically registered to the follow-up CT images. Tissue physical density change and radiation dose were computed for each voxel within each fibrosis volume and within normal lung. Patient responses were grouped per radiation and chemotherapy protocol.

RESULTS: A significant correlation was noted between fibrosis grade and tissue physical density change and fibrosis grade. For doses less than 30 Gy, the probability of observing fibrosis was less than 2% with conventional fractionation and less than 4% with accelerated fractionation. Physical lung density change also showed a threshold of 30–35 Gy. For doses of 30–55 Gy and cisplatin and etoposide (PE) chemotherapy, fibrosis probability was 2.0 times greater for accelerated fractionation compared with conventional fractionation ($P < .005$) and was correlated to increasing dose for both fractionation schedules.

CONCLUSION: Lung tissue physical density changes correlated well with fibrosis incidence, and both increased with increasing dose greater than a threshold of 30–35 Gy. With concurrent PE chemotherapy, fibrosis probability was twice as great with accelerated fractionation as with once-daily fractionation.

Concurrent chemotherapy and radiation therapy have been shown to improve survival in patients with limited small cell lung cancer. In a study by Turrisi et al (1), twice-daily accelerated fractionation compared with standard daily fractionation resulted in a higher survival rate. On the basis of the radiosensitivity of small cell lung cancer, it was expected that multiple small fractions would reduce damage and late effects in normal tissues. An increase in esophageal toxic reaction was observed but no increase in pulmonary toxic reaction. In a related study, Geara et al (2) examined fibrosis in a subset of the patients in the Turrisi et al study (1) and found a correlation between dose and fibrosis. In contrast with expectations, more severe fibrosis was found in the group that received accelerated fractionation.

The appearance of radiation pneumonitis and radiation fibrosis on computed tomo-

graphic (CT) images has been described as four separate patterns of consolidation (3–5). The first, a homogeneous slight increase in attenuation that uniformly involves the irradiated lung, represents diffuse minimal early radiation pneumonitis. The second pattern is a patchy consolidation contained within the irradiated lung. This consolidation does not conform to the radiation portal and is considered to represent nonhomogeneous radiation pneumonitis. The third pattern is a discrete consolidation conforming to the radiation portal but without uniform involvement. It may reflect focal organizing pneumonitis or fibrosis. The fourth pattern, more indicative of radiation fibrosis, is a solid consolidation conforming to and totally involving the irradiated portion of the lung. In several studies (6,7), the use of CT for quantifying radiation damage has been investigated. Van Dyk and Hill (6) and Nicholas and Down (7) assessed early and late radiation damage to mouse lung. Despite the physical limitations of CT measurements in mouse lung, the authors of both studies found that postirradiation attenuation changes coincided with changes in breathing rate. Nicholas and Down (7) also found a correlation between attenuation changes and marked microscopic changes in the lung.

In previous research at the University of Texas M. D. Anderson Cancer Center (2), 25 patients with limited small-cell carcinoma of the lung who had unequivocal complete responses to radiotherapy and chemotherapy, as determined with radiographic studies, were selected from two chemotherapy protocols. Only patients with complete responses were chosen to eliminate the effects of residual or recurrent disease on the radiographic appearance of the lung. Analysis of the data identified total dose and fractionation as factors influencing the severity of lung fibrosis. It was found that the risk for and severity of lung fibrosis increased with the total dose and the accelerated fractionation schedule.

We hypothesized that lung physical density changes as calculated from CT would correlate with physician-identified radiographic fibrosis and could be used as an objective measure of radiation damage. We also hypothesized that the incidence and severity of fibrosis and lung physical density changes would increase with dose. Thus, the purpose of our study was to evaluate the relationship between fibrosis, lung tissue physical density change, and radiation dose after concurrent chemotherapy and radiation therapy for limited small cell lung cancer.

MATERIALS AND METHODS

Between 1989 and 1994, the University of Texas M. D. Anderson Cancer Center participated in a cooperative prospective study in which twice-daily accelerated radiation therapy was compared with standard daily fractionation thoracic radiation therapy, both with concurrent chemotherapy (cisplatin and etoposide [PE]). Radiation was delivered by using conventional fractionation (1.8 Gy per fraction, 1 fraction per day, and 5 fractions per week for 5 weeks) or accelerated fractionation (1.5 Gy per fraction, 2 fractions per day with a 6-hour or greater interfractional interval, and 10 fractions per week for 3 weeks) for a total dose of 45 Gy. The PE chemotherapy protocol consisted of 60 mg/m^2 of intravenously administered cisplatin (Platinol-AQ; Bristol-Myers Squibb, Princeton, NJ) on day 1 and 120 mg/m^2 of orally administered etoposide (Vepesid; Bristol-Myers Squibb) on days 1–3. This regimen was repeated every 21 days for four cycles.

In a second prospective study in which twice-daily accelerated radiation therapy was performed, a modified chemotherapy protocol, cisplatin, ifosfamide, and etoposide (PIE), consisting of 20 mg/m^2 of intravenously administered cisplatin and 1,200 mg/m^2 of intravenously administered ifosfamide (Ifex; Bristol-Myers Squibb) on days 1–3 with 40 mg/m^2 of etoposide on days 1–14 was compared with the PE chemotherapy. Each patient received 240 mg/m^2 of mesna (Mesnex; Bristol-Myers Squibb) intravenously before initiation of ifosfamide administration and 480 mg/m^2 of mesna 4 hours after initiation of ifosfamide administration. This chemotherapy regimen was repeated every 28 days for four cycles. Eligibility criteria were the same for both protocols. Institutional review board approval and patient informed consent were obtained for both of these studies.

Fifty-six patients with limited small-cell lung cancer were enrolled in these protocols. Their disease was staged by performing CT of the chest and upper abdomen, chest radiography, laboratory testing, CT or magnetic resonance (MR) imaging of the brain, bone marrow examination, and review of pathologic specimens from the primary tumor. Twenty-five of these patients, all those with complete responses to chemotherapy and radiation, were selected for the current study. In these patients, abnormal appearance of the lung tissue on radiographs or CT scans could be unequivocally ascribed to fibrosis and not confused with persistent or recurrent disease. These patients were the same ones included in a previous study by Geara et al (2). Subsequently, one patient was excluded from the current study because he was treated with a tissue compensator for which the three-dimensional (3D) treatment planning (TP) system could not be used to reconstruct the delivered doses. Three other patients were excluded because their TP or follow-up CT images were not available in a digital format.

Of the 21 patients in the study, eight received conventional fractionated radiation therapy with PE chemotherapy. Thirteen patients received twice-daily accelerated radiation therapy, eight with PE chemotherapy and five with PIE chemotherapy. Radiation treatment consisted of opposed anteroposterior-posteroanterior (AP-PA) beams with 1.5–2.0-cm margins followed by reduced oblique opposed beams. With conventional fractionation, a dose of 39.6 Gy or 41.4 Gy was delivered with the AP-PA fields, and then 5.4 Gy or 3.6 Gy was delivered with the boost fields. Two patients were treated by using AP-PA fields only. With the accelerated treatment, a 30-Gy dose was delivered with the AP-PA beams, followed by 15 Gy with the boost fields. All patients underwent prophylactic irradiation of the brain with a 25-Gy dose given in 10 fractions over 2 weeks.

For all patients, CT was performed by using a HiLight Advantage scanner (GE Medical Systems, Milwaukee, Wis) with 10-mm sections. TP CT images were obtained through the treatment volume. Follow-up CT of the entire lung volume was performed immediately after treatment and then every 6 months. Fibrosis was evaluated on the 1-year follow-up CT images obtained at 10–16 months following therapy (median, 13 months).

Definition of Fibrosis Volumes

An experienced radiation oncologist (R.K.) in consultation with diagnostic radiologists examined each follow-up image for each patient and manually outlined fibrosis volumes by using the RTOG (Radiation Therapy Oncology Group) scoring system for late morbidity (Table 1) as a guide. Although the scoring system includes symptomatic criteria, only the radiographic ones were used. The RTOG scores for radiographs were applied to the CT images as follows: Grade 0 indicated no change in opacity; grade 1, slight opacity changes; grade 2, patchy opacity changes; and grade 3, dense

opacity changes. Figure 1 shows typical fibrosis volumes drawn on a single section. To minimize interpatient variations in scoring, window and level settings for all images were the same for all patients and as close as possible to the values used for the diagnostic hard copy images. Fibrosis volumes were identified according to grade assignment. Lung regions with no fibrosis (grade 0) were also outlined and identified as ipsilateral or contralateral. All five regions were treated as separate structures in the data analysis.

TABLE 1
RTOG/European Organization for Research and Treatment of Cancer Late Radiation Morbidity Scoring Scheme for Lung

Grade No.	Description
0	No change
1	Asymptomatic or mild symptoms (dry cough), slight radiographic appearance
2	Moderate symptomatic fibrosis or pneumonitis (severe cough), low-grade fever, patchy radiographic appearance
3	Severe symptomatic fibrosis or pneumonitis, dense radiographic changes
4	Severe respiratory insufficiency, oxygen requirement, assisted ventilation

Note.—From reference 8.

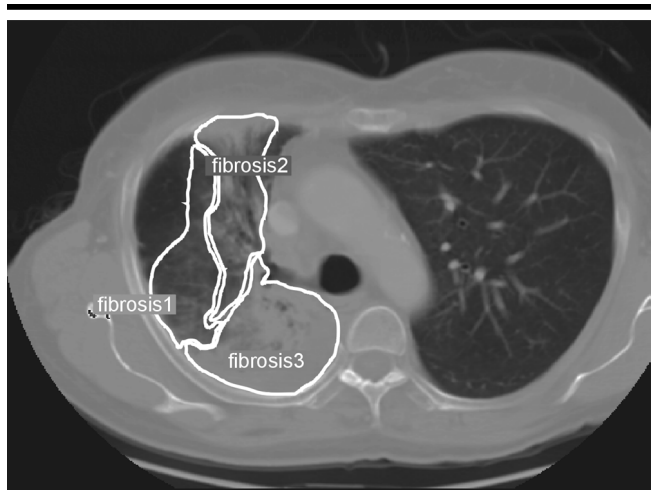

Figure 1. Transverse CT section shows typical fibrosis volumes.

Three-dimensional Reconstruction of Delivered Doses

The volumetric dose distribution delivered to each patient was reconstructed by using a 3D TP system, COPPER-Plan (9), developed at the University of Texas M. D. Anderson Cancer Center. The lungs, trachea, and spinal cord were outlined by using manual entry (T.A.F., R.K.). The skin surface, clavicles, and vertebrae were automatically outlined with the COPPER-Plan software by using threshold techniques and were then manually edited (T.A.F.), if needed. The shape of each radiation port was digitized into the system from the simulator image used for constructing treatment blocks. Beams were placed by aligning beam centers and edges with radiopaque catheters on the skin and by comparing beams-eye-view projections with simulator films (T.A.F., R.K., I.I.R.). The COPPER-Plan TP system used a 3D photon convolution algorithm for dose computation (10,11), and all doses were corrected for tissue density variations.

Geometric Registration of Data Sets

The follow-up images and corresponding TP images were geometrically registered by using an image alignment process based on the method of Antolak et al (12) (T.A.F., I.I.R.). All CT scans were obtained with the patient's head first as the patients lay in a supine position. The orientation of the coordinate system was +x toward the patient's left side, +z toward the patient's anterior side, and +y toward the patient's head. Transverse, sagittal, and coronal projection images were created for each examination. The follow-up images were interactively translated, scaled, and/or rotated until the best visual agreement with the TP images was obtained. Out-of-plane rotations about the patients' x (left-right) and z (anteroposterior) axes were assumed to be negligible and were omitted. Agreement was guided by matching lung tissue between image data sets rather than matching soft tissue, bone, or skin. During alignment, a 3D coordinate transformation matrix was maintained and updated after each change in the orientation or size of the follow-up data set.

Projection images were created in a two-step process. First, a portion of the 3D image data set was defined by setting clipping limits in each direction. Only voxels within the clipping volume were used to create the images. High and low threshold values for the CT numbers were defined to emphasize specific anatomy. To display only the lungs, the CT number thresholds were set at 100 and 800. To view the soft tissues, the CT number thresholds were set at 800 and 2,000. In computing the projection images, the contribution of each voxel was the smaller of [(CT number) − (low threshold)] or [(high threshold) − (CT number)]. For a sagittal image, CT numbers were summed along rows in the x (left-right) direction. For a coronal image, CT numbers were summed along columns in the z, or anteroposterior, direction. For a transverse projection image, a single transverse section was selected, and the threshold operation was applied to the pixels in that section. Each projection image was displayed at a resolution of 300 × 300 pixels by using 256 gray levels.

Image alignment started with coarse adjustment using a coronal-sagittal-transverse registration window (Fig 2). TP images were shown on the left, and corresponding follow-up images were shown on the right. A superimposed reference graticule aided in adjusting image size. The follow-up images were moved and scaled manually until the image sets were in approximate alignment. This window was always open, showing the current positions of the data sets.

A second window, the three transverse image window, showing three transverse projection images was then used to refine the alignment in the superior-inferior direction (Fig 3). The displayed transverse images were selected to represent superior, middle, and inferior regions through the lungs. Again, TP images were shown on the left, and corresponding follow-up images were shown on the right. The follow-up images were computed on the ba-

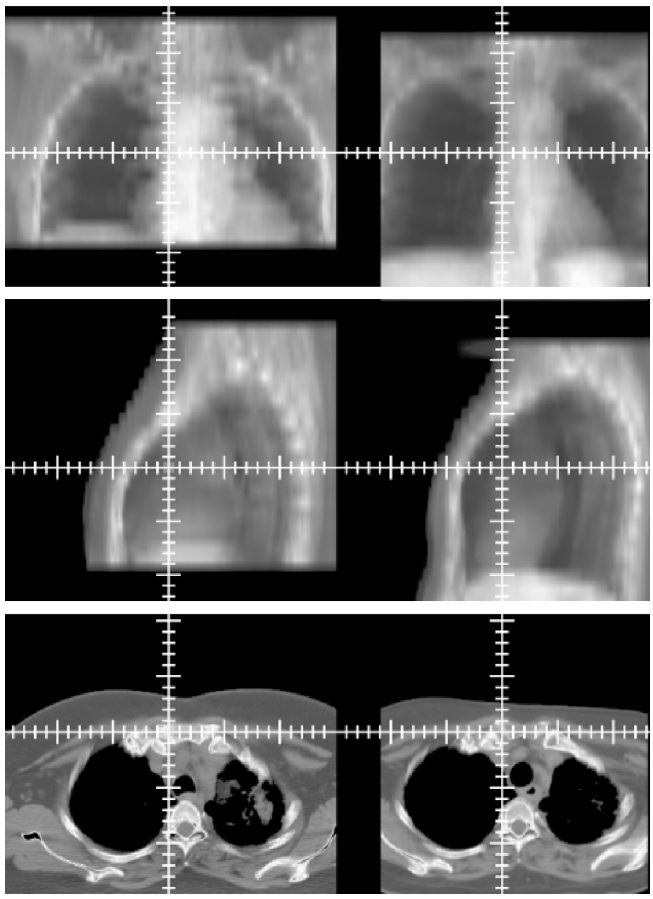

Figure 2. Example of the coronal-sagittal-transverse registration window (top to bottom) shows images after data set alignment. Left, TP images; right, corresponding follow-up images.

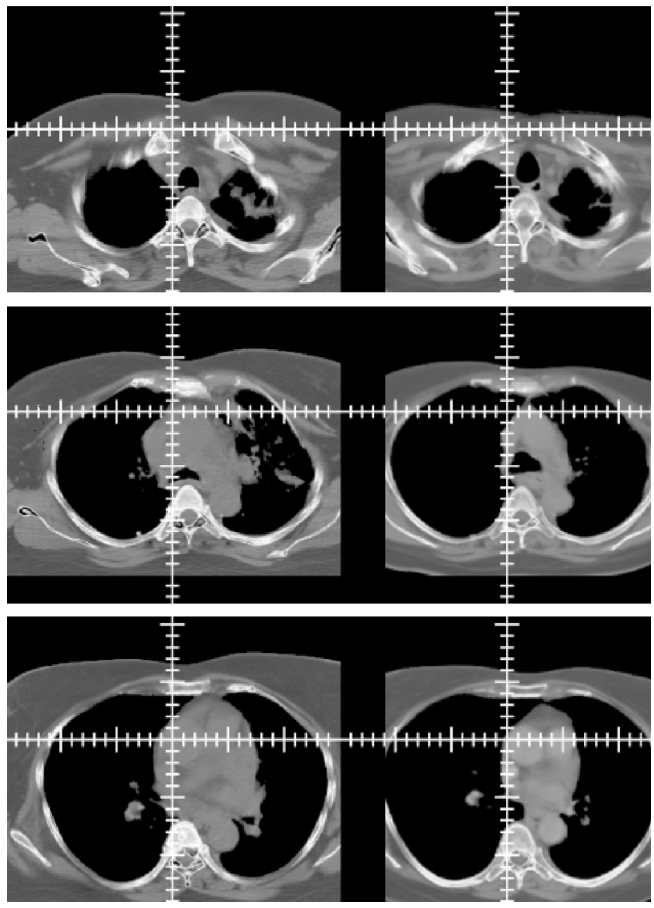

Figure 3. Example of the three transverse image registration windows shows images representing the superior, middle, and inferior regions of the lungs. Left, TP images; right, corresponding follow-up images. This display was used to verify or adjust alignment in the superior-inferior direction.

sis of the current value of the transformation matrix. Alignment along the y, or superior-inferior, direction was based on the locations of the head of the clavicle and of the sternum and carina.

Final adjustments were made by using an interactive alignment window that showed three composite transverse images in a horizontal panel (Fig 4). Follow-up images in yellow were superimposed onto TP images in gray. The position and orientation of the follow-up image data relative to the TP image data were modified interactively and displayed by using two presentations. In one presentation, thresholds were used to emphasize lung tissue in both image sets (Fig 4). In the second presentation, an edge image of the follow-up study was superimposed on a soft-tissue image of the TP study (Fig 5). Edge images (13) were computed by averaging central differences along the x and y directions:

$$F_E = \frac{1}{2}|\Delta_{2x} * f| + \frac{1}{2}|\Delta_{2y} * f|, \qquad (1)$$

where

$$\Delta_{2x} = [-1 \quad 0 \quad 1]$$

is the operator applied in the x direction,

$$\Delta_{2y} = \begin{bmatrix} 1 \\ 0 \\ -1 \end{bmatrix}$$

is the operator applied in the y direction, f is the input image, and F_E is the output edge image.

During alignment, translations were computed by changing the offset between the two images. Rotations were accomplished by using an algorithm that decomposes the two-dimensional rotation matrix into the product of three shear matrices (14). First, an image is skewed in the x direction. The resulting image is then skewed in the y direction. The final rotated image is obtained by skewing in the x direction again. For speed, only the projection images were changed during interactive alignment, not the entire underlying follow-up image data set. The individual adjustments were recorded by continuously updating a 4×4 transformation matrix. Periodically, new projection images were computed on the basis of the total transformation matrix to eliminate the accumulation of approximation errors. After alignment was completed, the follow-up image data and anatomy outlines were transformed to the TP coordinate system by using the final value of the 4×4 matrix. This produced a data set that contained the CT images, anatomy outlines, and doses in a single coordinate system.

Lung Physical Density Change versus Fibrosis

A physical density corresponding to each CT image voxel was computed from the attenuation value by using a look-up table calibrated to the CT scanner and x-ray energy (120 kVp). The original un-

transformed follow-up data sets were used to avoid the interpolations of CT values required in the geometric transformation process. The true lung physical density change resulting from irradiation, the difference in physical density in each voxel before and after irradiation, was impossible to measure. An approximation to the unirradiated baseline physical density value was measured (T.A.F.) for each patient by using the average physical density of voxels in the contralateral lung receiving less than 2 Gy. For each delineated fibrosis volume in each patient, an average fibrosis physical density was computed from the physical densities of the voxels in the volume. Then, for each patient, the lung tissue physical density change corresponding to each fibrosis grade was obtained by subtracting the baseline physical density from the average fibrosis volume physical density. Finally, tissue physical density changes for the individual patients were averaged to associate an average tissue physical density change with each fibrosis grade.

Tissue physical density changes were assigned to ranges corresponding to the different fibrosis grades. The physical densities associated with grade 0 (no fibrosis) ranged from 0 g/mL to 2 standard errors less than the mean physical density associated with grade 1 opacity. The physical densities associated with grade 1 opacity started at the upper end of the grade 0 range and ended halfway between the mean physical densities associated with grades 1 and 2 opacity. Similarly, the physical densities associated with grade 2 opacity started at the upper end of the grade 1 range and ended halfway between the mean physical densities associated with grades 2 and 3 opacity. The physical densities associated with grade 3 opacity started at the upper end of the grade 2 range and ended at 2 standard errors greater than the mean physical density associated with grade 3 opacity.

Probability of Fibrosis and Lung Density Change

For probability calculations, doses were aggregated into 5-Gy intervals. The probability of observing fibrosis as a function of dose was computed for each grade individually and for all grades together by using Equations 2 and 3 (Appendix). The probability of measuring a tissue physical density change of a given grade as a function of dose was computed for each patient for each grade individually and for all grades together by using Equations 4 and 5 (Appendix). At each dose level, probabilities were computed for the individual patients and then av-

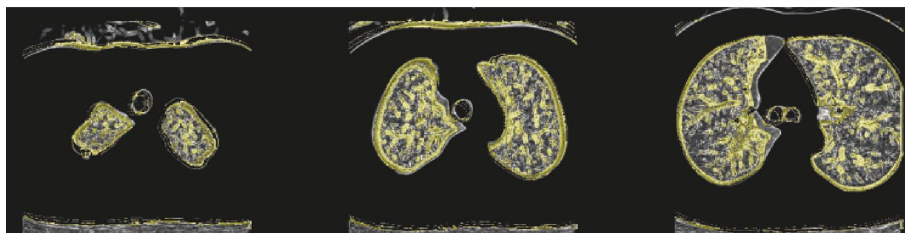

Figure 4. Example of the interactive alignment registration window used for final adjustment of the alignment between the follow-up and transverse TP images. In this example, thresholds were used to emphasize the lung tissue.

TABLE 2
Mean Tissue Physical Density Change in 21 Patients

Patient No.	Tissue Physical Density Change			Baseline Physical Density
	Grade 1	Grade 2	Grade 3	
3	0.223 ± 0.187	0.471 ± 0.206	0.739 ± 0.107	0.240
4	. . .	0.125 ± 0.133	0.566 ± 0.282	0.158
5	0.103 ± 0.164	0.225 ± 0.204	0.650 ± 0.152	0.258
6	. . .	0.591 ± 0.218	0.879 ± 0.127	0.201
7	0.137 ± 0.139	0.351 ± 0.218	0.774 ± 0.167	0.154
8	0.154 ± 0.176	0.448 ± 0.251	0.676 ± 0.193	0.193
9	0.205 ± 0.000	0.320 ± 0.229	0.728 ± 0.182	0.205
10	0.105 ± 0.109	0.408 ± 0.218	0.750 ± 0.101	0.207
11	0.300 ± 0.000	0.370 ± 0.228	0.704 ± 0.175	0.193
12	0.142 ± 0.151	0.427 ± 0.226	0.525 ± 0.000	0.246
13	0.119 ± 0.186	0.245 ± 0.223	0.693 ± 0.233	0.122
14	0.242 ± 0.196	0.527 ± 0.266	0.776 ± 0.000	0.176
15	0.242 ± 0.170	0.363 ± 0.233	0.638 ± 0.205	0.180
16	0.198 ± 0.145	0.500 ± 0.181	0.759 ± 0.089	0.225
17	0.198 ± 0.168	0.373 ± 0.228	0.745 ± 0.149	0.187
18	0.207 ± 0.169	0.358 ± 0.230	0.719 ± 0.171	0.194
19	0.171 ± 0.144	0.308 ± 0.189	. . .	0.171
21	0.261 ± 0.169	0.434 ± 0.205	0.720 ± 0.184	0.209
22	0.330 ± 0.091	0.484 ± 0.246	0.736 ± 0.179	0.156
23	0.242 ± 0.159	0.494 ± 0.235	0.701 ± 0.172	0.205
24	0.201 ± 0.151	0.311 ± 0.223	0.682 ± 0.094	0.194
Mean change	0.197 ± 0.037	0.361 ± 0.047	0.731 ± 0.034	0.194 ± 0.033

Note.—Data are for each physician-identified radiographic fibrosis grade for each patient and are in grams per milliliter. The baseline physical density is the average physical density of all voxels in the contralateral lung receiving less than 2 Gy. For individual patients, the SD is shown. For the sample mean, the standard error is given.

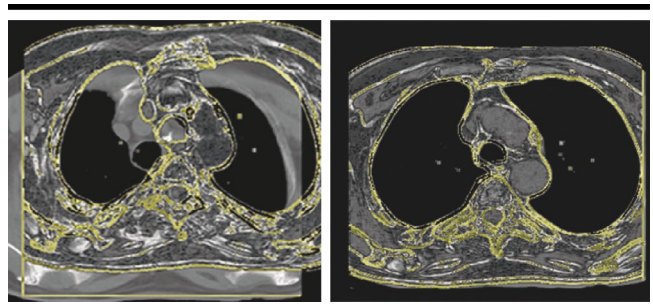

Figure 5. Example of the interactive alignment registration using a soft-tissue display of the transverse TP image and an edge display of the transverse follow-up image. Left, before alignment; right, after alignment.

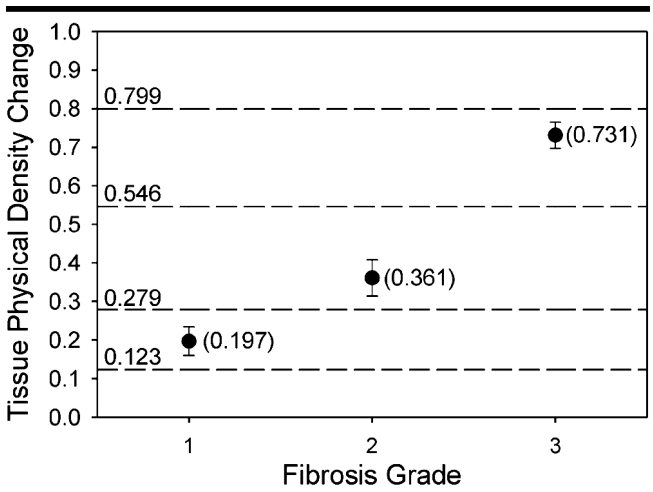

Figure 6. Graph shows the mean physical density change corresponding to each physician-identified radiographic fibrosis grade. Dashed lines separate ranges of tissue physical density changes associated with the different grades of fibrosis. Error bars = ±1 standard error.

eraged separately for each fractionation and chemotherapy combination.

Statistical Analysis

The relationship between tissue physical density change and physician-identified fibrosis grade was tested for statistical significance by using the Student *t* test. A *P* value of .05 was considered to be statistically significant. The probabilities of fibrosis and physical density change for the different treatment protocols were compared by using paired ratios.

RESULTS

The relationship between physician-identified radiographic fibrosis and measured change in tissue physical density is shown in Table 2. The mean physical density change within each fibrosis volume is shown for each patient and for the group as a whole. The large variation in physical density changes within each grade of fibrosis reflects the subjective nature of the scoring system. For the group as a whole, the physical density changes associated with fibrosis grades 1, 2, and 3 were 0.197 g/mL ± 0.037 (standard error), 0.361 g/mL ± 0.047, and 0.731 g/mL ± 0.034, respectively. The mean baseline physical density was 0.194 g/mL ± 0.033. The tissue physical density changes associated with the clinical grades were statistically different (Student *t* test, $P < .05$). The mean values and their uncertainties are also shown in Figure 6, along with the divisions between the physical density change grades. Physical density changes greater than 0.799 g/mL were considered to be anomalies resulting from inexact registration of TP and follow-up images.

For analysis, patients were divided into three treatment groups: conventional fractionation with PE chemotherapy ($n = 8$), accelerated fractionation with PE chemotherapy ($n = 8$), or accelerated fractionation with PIE chemotherapy ($n = 5$). Doses greater than 55 Gy were omitted because they occurred in only two patients.

Probability of Fibrosis

The probabilities of observing each grade of fibrosis individually (Eq [2]) and all grades combined (Eq [3]) are shown in Figure 7 as functions of dose for all patients individually. The large interpatient variability in response is evident. For several patients, the probability of fibrosis decreased unexpectedly at doses greater than 45 Gy because of the inexact alignment of the TP and follow-up images, missed voxels in the outlining process, or both.

For each dose level, the individual patient probabilities were averaged for the different fractionation and chemotherapy combinations (Fig 8 and Table 3). When the dose was limited to less than 30 Gy, the average probability of observing fibrosis was less than 2% for the conventional fractionation and less than 4% for the accelerated fractionation. At doses of 50–55 Gy, this probability increased to 24.7% for conventional fractionation, 55.0% for accelerated fractionation with PE chemotherapy, and 18.6% for accelerated fractionation with PIE chemotherapy. For doses of 30–55 Gy, the probability of fibrosis was correlated with increasing dose for the conventional fractionation plus PE chemotherapy combination ($r = 0.932$, $P_c \approx 0.02$) and for the accelerated fractionation plus PE chemotherapy combination ($r = 0.954$, $P_c \approx 0.01$), where P_c is the probability that the data are not correlated. Accelerated fractionation plus PIE chemotherapy showed a trend toward increasing probability of fibrosis with dose, but the correlation was not statistically significant, probably because of the small sample size.

For the patients receiving PE chemotherapy, fibrosis was more likely with accelerated fractionation. For doses of 30–55 Gy, the average probability of any grade fibrosis with the accelerated fractionation schedule was 2.00 ± 0.34 times higher than that with conventional fractionation, and this ratio was significantly greater than one (paired ratios, Student *t* test, $P < .005$). The probability of fibrosis from the accelerated fractionation plus PIE chemotherapy regimen more closely matched the conventional fractionation plus PE protocol but was not statistically different from either of the others.

Probability of Tissue Physical Density Change

The probabilities of observing tissue physical density changes showed patterns similar to those of the probabilities of observing fibrosis, but the differences between the fractionation chemotherapy combinations were not statistically significant. The probabilities for each grade individually (Eq [4]) and all grades combined (Eq [5]) as functions of dose are shown in Table 4 and Figure 9. For doses of 30–55 Gy, the probability of observing a physical density change increased with increasing dose, but the correlation was not statistically significant because of the large uncertainties. The probabilities of tissue physical density changes at doses greater than 30 Gy were not significantly different for the three treatment combinations (paired ratios, Student *t* test).

DISCUSSION

The probability of observing radiographic lung fibrosis in the current study was found to increase with dose greater than a threshold of 30–35 Gy, similar to the result reported by Geara et al (2),

which was an apparent threshold for fibrosis at 30–40 Gy. Geara et al (2) also found that for doses greater than 40 Gy, accelerated fractionation produced a higher incidence of grade 3 fibrosis compared with conventional fractionation. We used more accurate 3D alignment of the delivered dose to the follow-up images and separated the patients into three fractionation and chemotherapy schedules. Consequently, we found that the risk and severity of fibrosis depended on the chemotherapy, as well as on the fractionation and dose. For the PE chemotherapy, the probability of any grade fibrosis was twice as great for accelerated fractionation as for conventional fractionation. With PIE chemotherapy, the accelerated fractionation produced less fibrosis and more closely approximated the conventional fractionation with PE chemotherapy. The consistency of our results with those of Geara et al (2) is due in part to the use of the same patient data. In addition, we eliminated potential observer bias by having the fibrosis volumes delineated without concurrent knowledge of the dose distribution.

We found that the change in lung tissue physical density was strongly correlated with the grade of physician-identified radiographic fibrosis. It was expected that changes in tissue physical density would correlate better to dose than would physician-identified grade, but they did not. This is probably because lung tissue is not homogeneous. Bronchioles and associated blood vessels introduce soft-tissue opacities at all dose levels; these opacities fall in the grades 1 and 2 opacity ranges. We found many voxels that received doses less than 5 Gy and registered physical density changes in ranges corresponding to fibrosis. These voxels corresponded to normal unit physical density tissues in the lung (eg, the bronchi) and did not represent true physical density changes; they only appeared to have physical density changes because a single global baseline physical density value was used.

Delineation of fibrosis volumes on CT images is very difficult. Fibrosis volumes usually do not have sharply defined edges; this is especially true for the lower grades. Furthermore, the uninvolved lung often has an abnormal appearance because of concomitant disease or functional compensation for the involved lung. Consequently, the absolute physical density of fibrosis is not uniform among patients, and there are large variations in baseline physical density (0.122–0.258 g/mL in the current study).

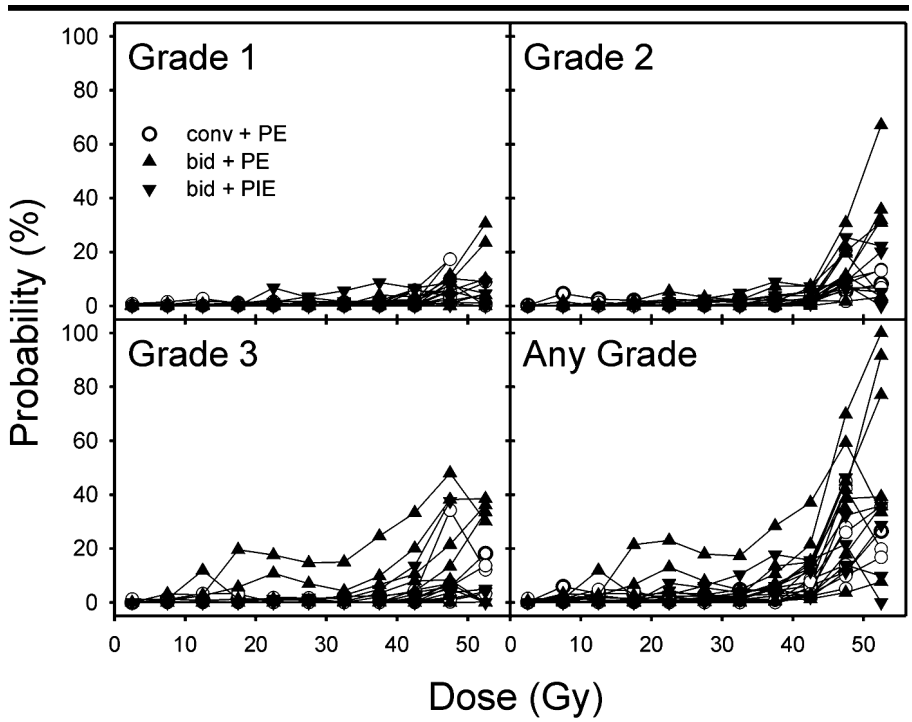

Figure 7. Graph shows the probability of physician-identified radiographic grade 1, 2, or 3 fibrosis or any fibrosis as a function of dose for each patient. The large interpatient response variability is evident. For several patients, the probability of fibrosis unexpectedly decreased at doses greater than 45 Gy because of the inexact alignment of the TP and follow-up images, missed voxels in the outlining process, or both. *bid* = twice-daily treatment, *conv* = conventional (once-daily) treatment.

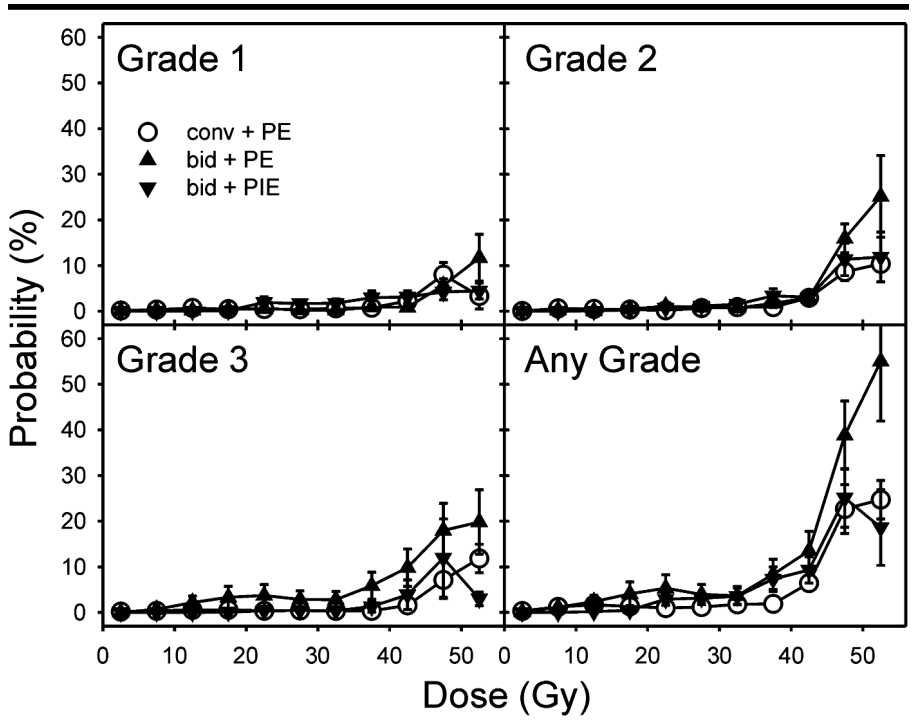

Figure 8. Graph shows the average probability of occurrence of physician-identified radiographic grade 1, 2, or 3 fibrosis or any fibrosis as a function of dose for each fractionation and chemotherapy combination. For doses of 30–55 Gy and PE chemotherapy, the risk of fibrosis (any grade) with the accelerated fractionation schedule was 2.01 ± 0.34 times higher than that with conventional fractionation ($P < .005$). The probability of fibrosis with the PIE chemotherapy was not statistically different from either of the other schedules. *bid* = twice-daily treatment, *conv* = conventional (once-daily) treatment. Error bars = ±1 standard error.

TABLE 3
Mean Probabilities of Fibrosis for Highest Dose Levels

Dose (Gy)	Probability of Fibrosis, any Grade*: Conventional Fractionation + PE (n = 8)	Accelerated Fractionation + PE (n = 8)	Accelerated Fractionation + PIE (n = 5)
30.0–34.9	1.8 ± 0.6	3.7 ± 2.0	3.6 ± 1.8
35.0–39.9	1.9 ± 0.8	8.4 ± 3.3	7.3 ± 2.7
40.0–44.9	6.4 ± 1.2	13.5 ± 4.3	9.3 ± 2.9
45.0–49.9	22.7 ± 5.3	38.8 ± 7.5	25.1 ± 6.4
50.0–54.9	24.7 ± 5.9	55.0 ± 13.1	18.6 ± 8.3

Note.—Patients are separated into three groups according to fractionation and chemotherapy.
* Means ± standard errors are percentages.

TABLE 4
Mean Probabilities of Physical Density Changes for the Highest Dose Levels

Dose (Gy)	Probability of Physical Density Change, any Grade*: Conventional Fractionation + PE (n = 8)	Accelerated Fractionation + PE (n = 8)	Accelerated Fractionation + PIE (n = 5)
30.0–34.9	5.8 ± 1.2	6.2 ± 2.5	8.3 ± 2.3
35.0–39.9	7.5 ± 1.2	5.6 ± 2.9	13.0 ± 3.1
40.0–44.9	12.8 ± 1.4	8.9 ± 3.4	15.8 ± 2.9
45.0–49.9	17.9 ± 3.3	24.9 ± 6.9	22.7 ± 2.8
50.0–54.9	17.5 ± 3.9	42.4 ± 12.8	28.1 ± 1.1

Note.—Patients are separated into three groups according to fractionation and chemotherapy.
* Means ± standard errors are percentages.

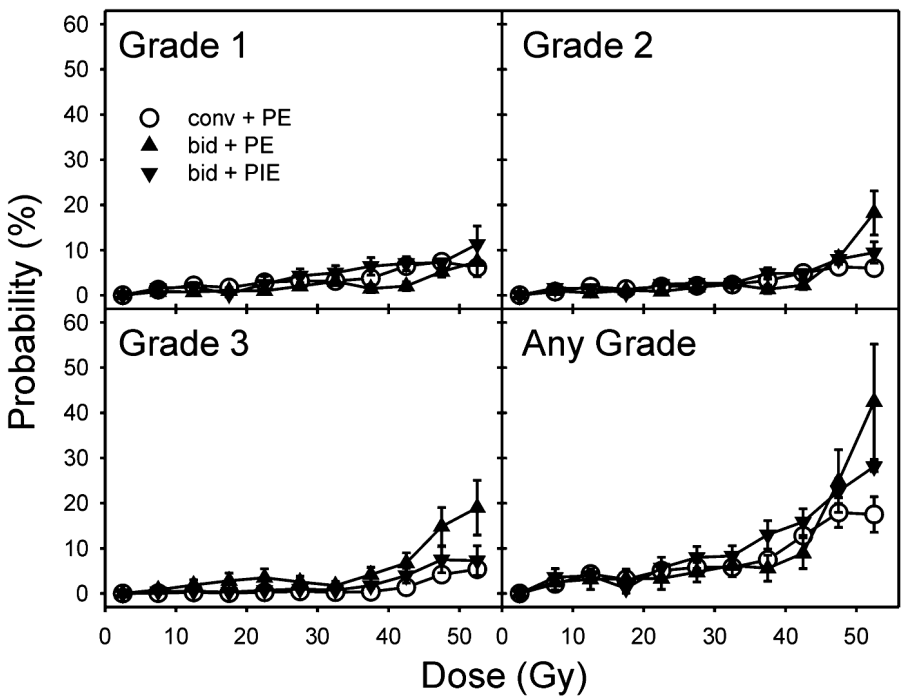

Figure 9. Graph shows the probability of measuring a given physical density change as a function of dose for each fractionation and chemotherapy schedule. The results for the three combinations are not statistically different. The probability of observing a physical density change becomes significant above a threshold of 30–35 Gy. *bid* = twice-daily treatment, *conv* = conventional (once-daily) treatment. Error bars = ±1 standard error.

The accuracy of correspondence between dose and effect (incidence of fibrosis and degree of tissue physical density change) depends on the accuracy of the registration process. Some difficulties in aligning pretreatment lung volumes with posttreatment lung volumes are unavoidable. They arise from changes in the anatomy caused by tumor shrinkage, contraction of normal tissues (eg, lung parenchyma and pleura) from the radiation-induced fibrosis, and compensatory changes in uninvolved and/or untreated lung tissue. Other alignment problems existed for the patients in the current study. The follow-up images were not obtained with the patient in the treatment position, the TP images did not always include the entire lung volume, and different breathing methods were used during scan acquisition. It appeared that the benefits of computer-assisted 3D registration of dose to anatomy did not compensate for the inherent differences in the image sets and the large interpatient variations.

In conclusion, tissue physical density changes computed from CT correlated well with physician-identified radiographic fibrosis, and both increased with increasing dose greater than a threshold of 30–35 Gy. With concurrent PE chemotherapy, the probability of fibrosis after radiation therapy for limited small-cell lung cancer was twice as great with accelerated fractionation as with once-daily fractionation.

APPENDIX

Probabilities of Fibrosis

The probability of observing a specific grade of clinical fibrosis was calculated as a function of dose based on voxel counts as follows:

$$P(\mathrm{F_i}, d) = \text{the probability of observing fibrosis grade } i \text{ from dose } d = N(\mathrm{F_i}, d)/N(\mathrm{T}, d) \quad \text{(A1)}$$

$$P(\mathrm{F_T}, d) = \text{the probability of observing any fibrosis from dose } d = \sum_{i=1}^{3} \mathrm{P}(\mathrm{F_i}, d), \quad \text{(A2)}$$

where $N(\mathrm{F_i}, d)$ = the number of voxels in fibrosis volume of grade i receiving dose d, and $N(\mathrm{T}, d)$= the total number of voxels in the lung receiving dose d. Doses were aggregated into 5-Gy intervals starting at 0 Gy.

Probabilities of Lung Physical Density Change

The probability of measuring a specific grade of lung physical density change was calculated as a function of dose on the basis of voxel counts as follows:

$$P(\Delta\rho_i, d) = \text{the probability of measuring a lung physical density change of grade } i \text{ from dose } d = N(\Delta\rho_i, d) / N(T, d) \quad \text{(A3)}$$

$$P(\Delta\rho_T, d) = \text{the probability of observing a physical density change of any grade from dose } d = \sum_{i=1}^{3} P(\Delta\rho_i, d), \quad \text{(A4)}$$

where $N(\Delta\rho_i, d)$= the number of voxels with physical density change of grade i receiving dose d.

Doses were aggregated into 5-Gy intervals starting at 0 Gy.

References

1. Turrisi AT, Kyungmann K, Blum R, et al. Twice-daily compared with once-daily thoracic radiotherapy in limited small-cell lung cancer treated concurrently with cisplatin and etoposide. N Engl J Med 1999; 340:265–271.
2. Geara FB, Komaki R, Tucker SL, Travis EL, Cox JD. Factors influencing the development of lung fibrosis after chemoradiation for small cell carcinoma of the lung: evidence for inherent interindividual variation. Int J Radiat Oncol Biol Phys 1998; 41:279–286.
3. Libshitz HI. Radiation changes in the lung. Semin Roentgenol 1993; 28:303–320.
4. Davis SD, Yankelevitz DF, Henschke Cl. Radiation effects on the lung: clinical features, pathology, and imaging findings. AJR Am J Roentgenol 1992; 159:1157–1164.
5. Libshitz HI, Shuman LS. Radiation-induced pulmonary change: CT findings. J Comput Assist Tomogr 1984; 8:15–19.
6. Van Dyk J, Hill RP. Post-irradiation lung density changes measured by computerized tomography. Int J Radiat Oncol Biol Phys 1983; 9:847–852.
7. Nicholas D, Down JD. The assessment of early and late radiation injury to the mouse lung using x-ray computerised tomography. Radiother Oncol 1985; 4:253–263.
8. Cox JD, Stetz J, Pajak TF. Toxicity criteria of the Radiation Therapy Oncology Group (RTOG) and the European Organization for Research and Treatment of Cancer (EORTC). Int J Radiat Oncol Biol Phys 1995; 31:1341–1346.
9. Starkschall G, Bujnowski S, Wang L, et al. A full three-dimensional radiotherapy treatment planning system (abstr). Med Phys 1991; 18:647.
10. Boyer AL, Mok EC. Calculation of photon dose distributions in an inhomogeneous medium using convolutions. Med Phys 1986; 13:503–509.
11. Zhu Y, Boyer AL, Desobry GE. Dose distributions of x-ray fields as shaped with multileaf collimators. Phys Med Biol 1992; 37:163–174.
12. Antolak JA, Rosen II, Childress CH, Zagars GK, Pollack A. Prostate target volume variations during a course of radiotherapy. Int J Radiat Oncol Biol Phys 1998; 42:661–672.
13. Rosenfeld A, Kak AC. Digital picture processing. Vol 2. Orlando, Fla: Academic Press, 1982.
14. Paeth A. A fast algorithm for general raster rotation. In: Glassner A, ed. Graphic gems. Cambridge, Mass: Academic Press Professional, 1990; 179–190.